THE JOURNAL OF PHYSICAL CHEMISTRY A

ARTICLE

pubs.acs.org/JPCA

Nonadiabatic Decomposition of Gas-Phase RDX through Conical Intersections: An ONIOM-CASSCF Study

A. Bhattacharya† and E. R. Bernstein*

Department of Chemistry, Colorado State University, Fort Collins, Colorado 80521, United States

ABSTRACT: Topographical exploration of nonadiabatically coupled ground- and excited-electronic-state potential energy surfaces (PESs) of the isolated RDX molecule was performed using the ONIOM methodology: Computational results were compared and contrasted with the previous experimental results for the decomposition of this nitramine energetic material following electronic excitation. One of the N−NO_2 moieties of the RDX molecule was considered to be an active site. Electronic excitation of RDX was assumed to be localized in the active site, which was treated with the CASSCF algorithm. The influence of the remainder of the molecule on the chosen active site was calculated by either a UFF MM or RHF QM method. Nitro−nitrite isomerization was predicted to be a major excited-electronic-state decomposition channel for the RDX molecule. This prediction directly corroborates previous experimental results obtained through photofragmentation-fragment detection techniques. Nitro−nitrite isomerization of RDX was found to occur through a series of conical intersections (CIs) and was finally predicted to produce rotationally cold but vibrationally hot distributions of NO products, also in good agreement with the experimental observation of rovibrational distributions of the NO product. The ONIOM (CASSCF:UFF) methodology predicts that the final step in the RDX dissociation occurs on its S_0 ground-electronic-state potential energy surface (PES). Thus, the present work clearly indicates that the ONIOM method, coupled with a suitable CASSCF method for the active site of the molecule, at which electronic excitation is assumed to be localized, can predict hitherto unexplored excited-electronic-state PESs of large energetic molecules such as RDX, HMX, and CL-20. A comparison of the decomposition mechanism for excited-electronic-state dimethylnitramine (DMNA), a simple analogue molecule of nitramine energetic materials, with that for RDX, an energetic material, was also performed. CASSCF pure QM calculations showed that, following electronic excitation of DMNA to its S_2 surface, decomposition of this molecule occurs on its S_1 surface through a nitro−nitrite isomerization producing rotationally hot and vibrationally cold distributions of the NO product.

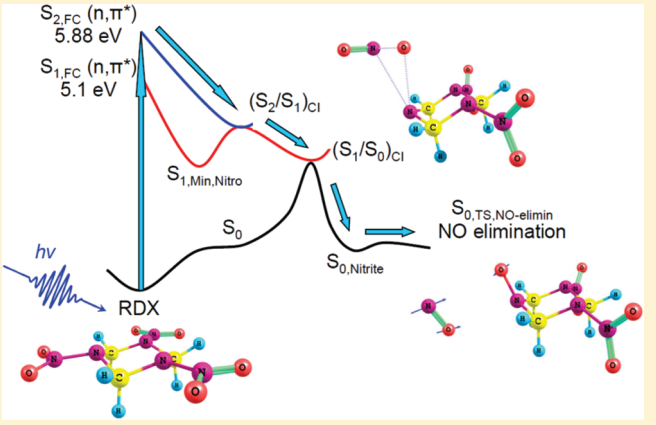

I. INTRODUCTION

Excited electronic states of RDX (1,3,5-trinitro-1,3,5-triazacyclohexane; see structure in Figure 1), generated through all kinds of ignition processes, such as sparks, shocks, heat, arcs, and compression waves, have been shown to be important in the initial step of decomposition of this energetic material.[1−14] Electronic excitation in this solid nitramine explosive under shock or compression waves is proposed to occur through several accepted mechanisms, including decreased energy gap between the highest occupied molecular orbital (HOMO) and lowest unoccupied molecular orbital (LUMO),[5] promotion of lattice defects,[6] shearing of crystal planes, and initiation of hole migration across the crystal. To understand fully how the chemical energy in RDX converts into mechanical energy through excited-electronic-state decomposition, the specific topography of the excited-electronic-state potential energy surfaces (PESs) of RDX, which eventually determines and controls the pathway for its decomposition, must be explored and understood.[15]

Exploration of excited-electronic-state PESs of large energetic nitramine molecules such as RDX is not directly feasible using only conventional quantum mechanical (QM) methodologies, which can describe an excited state with adequate accuracy.[15] In general, multiconfiguration-based ab initio QM methods, such as complete-active-space self-consistent field (CASSCF) and CAS perturbation theory (CASMP2/CASPT2) are more accurate for exploring excited-electronic-state PESs but are still too expensive to apply to large energetic molecules such as RDX. The requirement of a very large active space to perform the CASSCF calculation for RDX further complicates the effort. In that case, reduction of the active space does not solve the problem; rather, it introduces spurious effects into the computational results. Less expensive QM methods, such as time-dependent density functional theory (TDDFT) and configuration interaction singles

Received: September 24, 2010
Revised: March 17, 2011
Published: April 11, 2011

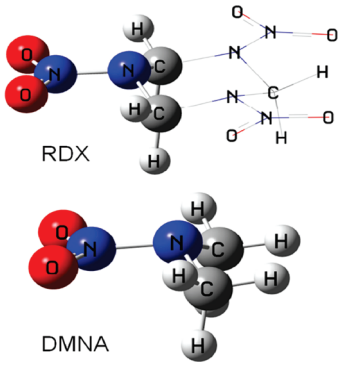

Figure 1. Schematic structures of RDX and DMNA. The high-level region of RDX is depicted by balls, and the low-level region is depicted by a wire frame. Here, electronic excitation in the RDX molecule is assumed to be localized entirely in the active site (more specifically in one N−NO_2 moiety) of the molecule.

(CIS), are not as accurate but are faster; however, they might not be fast enough for really large energetic molecular systems such as RDX.

Over the years, a variety of hybrid methods[16] have been presented that, in principle, offer a solution to the above scaling problem that arises because of a conflict between accuracy of results and computational costs. The most suitable hybrid method for exploring excited electronic PESs of RDX should have the ability to calculate relaxation paths associated with all possible photophysical processes, such as internal conversion and intersystem crossing through conical intersections (CIs) and different photochemical channels.[15] "Our own *N*-layered integrated molecular orbital and molecular mechanics" (ONIOM) method, developed by Morokuma and co-workers,[17] is an efficient hybrid scheme that has been demonstrated to be capable of efficiently exploring excited-electronic-state processes of large molecules.[18,19]

The ONIOM methodology combines different levels of theory for different parts of a large molecular system. More details of this methodology are discussed in the Computational Method section. The basic idea results in the realization that, for a large molecule, photochemical and photophysical processes are often localized only in a segment (called active site) of the molecule; the effect of the rest of the molecule on this moiety can often be only steric or electrostatic. Therefore, the photophysical or photochemical processes being investigated, localized at the active site, can be treated at an appropriate high-accuracy multiconfiguration QM method (e.g., CASSCF), whereas the remainder of the molecule can be treated with a lower level of theory [e.g., Hartree−Fock (HF) quantum mechanics (QM) or universal force field (UFF) molecular mechanics (MM)]. In this way, one can avoid unnecessary computational effort.

To apply the ONIOM methodology to the RDX system, one of the N−NO_2 in RDX moieties is considered to be the active site, and electronic excitation is assumed to be localized entirely in the active site. This approximation excludes the possible role of charge-transfer (CT) states (between nitramine moieties) in the overall description of excited electronic PESs of the large RDX molecule. Here, we apply the ONIOM methodology coupled with a CASSCF algorithm to explore excited-electronic-state PESs of RDX employing an assumption of local excitation. The assumption of local excitation in the RDX molecule was tested against experimental results; it was not tested computationally in this

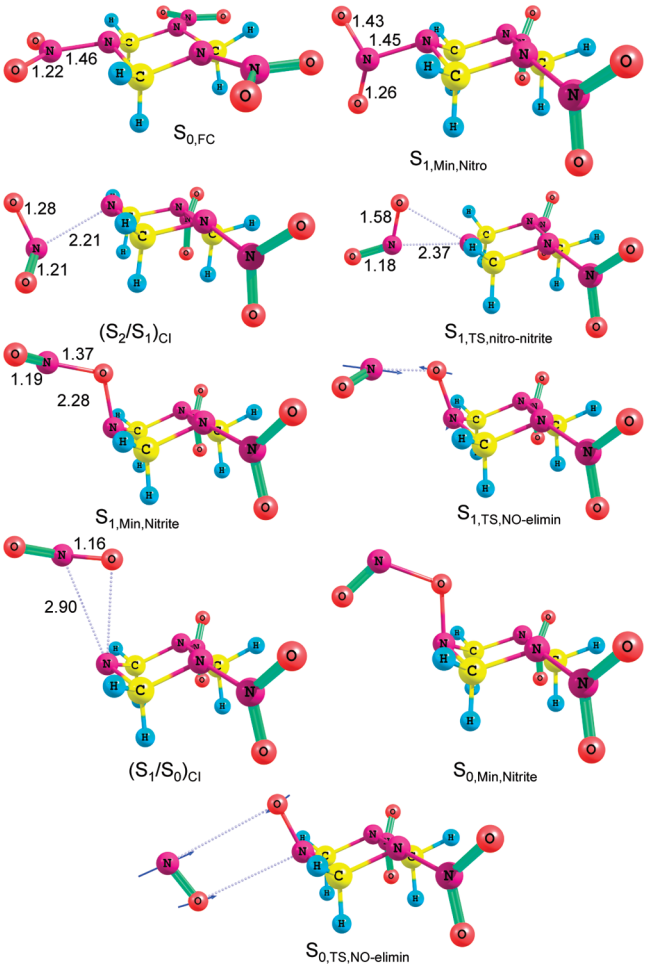

Figure 2. Structures of RDX at different critical points on PESs optimized at the ONIOM[CAS(10,7)/6-31G(d):UFF] level of theory. Blue arrows indicate the unstable normal mode of vibration associated with the respective transition state. Bond lengths are indicated for the active site.

work. Therefore, a comparison of the theoretical results with previous experimental results was performed to provide many mechanistic details of the decomposition of excited-electronic-state RDX and to provide a realistic justification of the applicability of the ONIOM method with the aforementioned assumption for the exploration of hitherto-unknown excited-state PESs of large energetic systems, such as HMX (octahydro-1,3,5,7-tetranitro-1,3,5,7-tetrazocine), CL-20 (2,4,6,8,10,12-hexanitro-2,4,6,8,10,12-hexaazaisowurtzitane), and so on. Because the experimental results of excited-electronic-state decomposition of RDX were presented in our previous publications,[20] only a summary of the experimental results is provided below.

IA. Previous Experimental Results. Unimolecular decomposition of isolated, excited-electronic-state RDX was previously studied by a photofragmentation-fragment detection scheme.[20] In this scheme, gas-phase RDX molecules are excited to an excited electronic state by absorption of a single UV photon of one of the four excitation wavelengths: 226, 236, 248, and 258 nm. As a result, the parent RDX molecule decomposes into products through certain decomposition pathways or channels. The fragments are then probed using energy-resolved optical spectroscopy [laser-induced fluorescence (LIF)] or mass-resolved

spectrometry [time-of-flight mass spectrometry (TOFMS), resonance-enhanced multiphoton ionization (REMPI)], which provide detailed internal-state (rotational and vibrational) energy distributions of the products. Such information clearly reflects the forces or torques that act on the departing fragments produced in the decomposition of excited-electronic-state RDX through a unique pathway. The internal-energy/-state distributions of the products ultimately lead to a proposed decomposition mechanism for the energetic material. Dynamics of the decomposition reaction are measured by femtosecond time-resolved pump−probe spectroscopy.

NO is observed to be the only initial product from the UV single-photon-induced photodissociation of RDX at 226, 236, 248, and 258 nm. NO is observed to be vibrationally hot (1800 K) and rotationally cold (20 K). OH is not observed to be a product from the decomposition of excited-electronic-state RDX. This result eliminates possible involvement of an HONO channel in the decomposition of excited-electronic-state RDX. Based on the energy-resolved spectroscopic signature for the NO product from RDX and other nitramine energetic materials such as HMX and CL-20, the dissociation mechanism for these energetic molecules is proposed to involve a nitro−nitrite isomerization. Observation of a vibrationally hot (∼1800 K) NO product from decomposition of excited-electronic-state RDX suggests that this energetic nitramine molecule dissociates on its ground-electronic-state PES after rapid internal conversion from upper excited electronic states. Details of this relaxation path, however, are unknown. The decomposition dynamics of molecules following electronic excitation at 226 nm is determined to be faster than 180 fs.[20c] Such fast decomposition dynamics are indicative of an almost barrierless dissociative excited-electronic-state PES of RDX; theoretical corroboration of this conclusion, however, has not been provided thus far.

IB. Current Work. Although the gas-phase unimolecular decomposition experiments performed to date suggest nitro−nitrite isomerization followed by NO elimination as the major decomposition channel of excited-electronic-state RDX,[20] a detailed mechanistic understanding of this reaction has, thus far, not been presented. The reason for generation of rotationally cold (20 K) NO products following decomposition of excited-electronic-state RDX also remains unexplained. Current understanding of photochemical dynamics suggests that decomposition of electronically excited nitramine species should occur through one or a number of conical intersections (CIs) involving different adiabatic PESs. This was demonstrated by our previous studies of dimethyl nitramine (DMNA; see Figure 1);[15] however, the role of nonadiabatic chemistry through CIs for the initial steps in the decomposition of true energetic species, such as RDX, HMX, and CL-20, has not been previously investigated. Therefore, the aim of the present work was to explore the mechanistic details of decomposition of electronically excited RDX using the ONIOM methodology. In particular, our focus included exploration of the nitro−nitrite isomerization pathway, the role of CIs in this process, internal energy distribution for the product NO, and the details of the excited-electronic-state PESs involved in the decomposition process. These mechanistic details were studied using the ONIOM methodology coupled with a CASSCF algorithm for the $N-NO_2$ active site. A comparison between the photochemical behavior of DMNA, a model energetic nitramine, and RDX, a true energetic nitramine molecule, is also presented. Finally, we address the question of why DMNA is not an energetic species, whereas RDX is.

II. COMPUTATIONAL METHOD

In the ONIOM method, a large molecular system is divided into two or three regions that are treated with different levels of theory. The results are then combined into the final predictions. This enables study of large molecular systems with less computational effort. The Gaussian 09 package[21a] can combine any two or three QM and MM computational methodologies into one calculation. In the current work, we considered two-layer QM:QM and QM:MM combinations, for which the total energy of a molecule is expressed through an extrapolation scheme as

$$E^{\mathrm{ONIOM}} = E^{\mathrm{High}}_{\mathrm{active\ site}} + E^{\mathrm{Low}}_{\mathrm{real}} - E^{\mathrm{Low}}_{\mathrm{active\ site}}$$

Here, active site denotes a small part of the real molecule, at which a chemical or physical process being studied is localized. An adequate high level is employed to describe accurately the behavior of the active site. A low-level and cheaper QM or MM method is employed for the full molecule (denoted as real). As a consequence, the active site is treated with both high and low levels of theory, and the full molecule is treated with only a low level of theory—this results in a "low-level region" that is outside the active site. The energy gradient is the derivative of the above expression with respect to the reaction coordinate, and the optimization is performed on the total PES gradient. The $(E^{\mathrm{Low}}_{\mathrm{real}} - E^{\mathrm{Low}}_{\mathrm{active\ site}})$ term in the ONIOM energy expression describes both the contribution from the low-level region and the interaction between the high- and low-level regions. In other words, coupling between the two regions is evaluated at a low computational level of theory. In general, the ONIOM method cannot calculate the absolute energy of the real system, as the various subcalculations (MM) either have different energy scales or are less accurate on the same energy scale (pure QM); however, the energy difference between two points on a PES will be reproduced with considerable accuracy.[17]

The active site and the remainder of the RDX molecule considered for the present work are illustrated in Figure 1. The high-level region is depicted by balls, and the low-level region is depicted by a wire frame. Here, electronic excitation was assumed to be localized entirely in the active site (more specifically in one $N-NO_2$ unit) of the molecule. Note the apparent similarity between DMNA and the RDX active site. The CASSCF algorithm (to calculate $E^{\mathrm{High}}_{\mathrm{active\ site}}$) was selected to treat the active site because this approach can successfully describe excited electronic states with adequate accuracy. Choice of a low-level method (to calculate $E^{\mathrm{Low}}_{\mathrm{real}} - E^{\mathrm{Low}}_{\mathrm{active\ site}}$) is not straightforward, however. Based on the assumption that electronic excitation is completely localized in the high-level region (active site), one can choose a ground-state method (e.g., HF, UFF), because the electronic excitation is the same in $E^{\mathrm{Low}}_{\mathrm{real}}$ and $E^{\mathrm{Low}}_{\mathrm{active\ site}}$ and therefore cancels in the difference $(E^{\mathrm{Low}}_{\mathrm{real}} - E^{\mathrm{Low}}_{\mathrm{active\ site}})$. Under this justification, however, the interaction between the high- and low-level regions would be based on the ground-state electronic structure, which might not be correct. For the present study, low-level ground-state methods, such as HF QM or UFF MM, were employed for calculation of the properties of the remainder of the RDX molecule. The difference of interaction energies between the high- and low-level regions related to the ground- and excited-electronic-state structures of RDX was assumed to be negligible. This assumption was justified through comparison of experimental and computational results and can be tested explicitly following the procedure given in ref 19.

Table 1. Geometrical Parameters of RDX at the ONIOM[CAS(10,7)/6-31G(d):UFF], MP2/6-31G(d), and ONIOM-[CAS(10,7)/6-31G(d):RHF/6-31G(d)] Levels of Theory

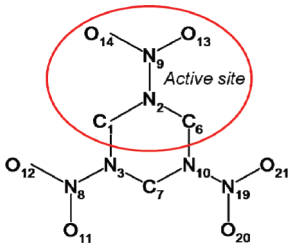

	A. ONIOM[CASSCF(10,7)/6-31G(d):UFF] FC/minimum/CI/TS							
	$S_{0,FC}$	$S_{1,Min,nitro}$	$(S_2/S_1)_{CI}$	$(S_1/S_0)_{CI}$	$S_{0,nitrite}$	$S_{1,Min,nitrite}$	$S_{1,TS}$	$S_{0,TS}$
				Bond Lengths (Å)				
N_9O_{14}	1.22	1.26	1.21	1.16	1.15	1.19	1.18	1.18
N_9N_2	1.46	1.45	2.21	2.90	2.44	2.28	2.37	3.35
N_9O_{13}	1.22	1.43	1.28	1.50	1.50	1.37	1.58	3.00
C_1N_2	1.46	1.46	1.43	1.45	1.46	1.46	1.45	1.47
C_6N_2	1.46	1.46	1.46	1.49	1.49	1.46	1.45	1.47
N_8O_{11}	1.21	1.20	1.21	1.21	1.21	1.21	1.21	1.21
N_8N_3	1.41	1.41	1.41	1.41	1.41	1.41	1.41	1.41
C_1N_3	1.46	1.46	1.47	1.46	1.46	1.46	1.46	1.47
C_7N_3	1.47	1.47	1.47	1.47	1.47	1.47	1.47	1.47
$N_{19}O_{20}$	1.21	1.21	1.21	1.21	1.20	1.20	1.21	1.20
$N_{10}N_{19}$	1.41	1.41	1.41	1.41	1.41	1.41	1.41	1.41
C_6N_{10}	1.46	1.46	1.46	1.46	1.46	1.46	1.46	1.47
C_7N_{10}	1.47	1.47	1.47	1.47	1.47	1.47	1.47	1.47
				Bond Angles (deg)				
$O_{14}N_9O_{13}$	126.3	110.6	118.5	110.7	115.4	102.9	112.9	81.88
$O_{14}N_9N_2$	116.7	122.9	104.8	103.6	81.71	114.6	101.3	58.65
$C_1N_2N_9$	111.5	110.2	98.94	100.4	124.7	124.8	123.0	118.3
$C_6N_2N_9$	111.5	108.2	102.7	126.3	116.1	115.8	121.3	117.6
$O_{12}N_8O_{11}$	119.4	119.4	119.2	119.4	119.4	119.4	119.4	119.4
$O_{11}N_8N_3$	121.2	121.3	121.8	119.4	119.4	119.4	119.4	121.2
$C_1N_3N_8$	109.9	109.9	110.2	109.8	109.7	109.7	109.8	109.3
$O_{20}N_{19}O_{21}$	119.4	119.4	119.2	119.4	119.4	119.4	119.4	119.4
$O_{20}N_{19}N_{10}$	121.2	121.2	122.1	119.4	119.4	119.4	119.4	121.2
$C_6N_{10}N_{19}$	109.9	109.9	110.8	109.8	109.7	109.8	109.8	109.7
				Dihedral Angles (deg)				
$O_{13}N_9N_2C_6$	22.0	154.3	102.7	29.3	82.0	83.69	86.9	108.3
$O_{11}N_8N_3C_1$	−12.0	61.3	65.7	118.83	119.1	119.0	118.9	−61.2
$O_{20}N_{19}N_{10}C_6$	12.0	61.5	63.4	−119.1	−119.0	−119.0	−119	61.3

	B. MP2/6-31G(d) and ONIOM[CAS(10,7)/6-31G(d):RHF/6-31G(d)] $S_{0,FC}$	
	MP2/6-31G(d)	ONIOM[CASSCF(10,7)/6-31G(d):RHF/6-31G(d)]
	Bond Lengths (Å)	
N_9O_{14}	1.24	1.23
N_9N_2	1.41	1.42
N_9O_{13}	1.24	1.19
C_1N_2	1.46	1.45

dx.doi.org/10.1021/jp109152p |J. Phys. Chem. A 2011, 115, 4135–4147

Table 1. Continued

	B. MP2/6-31G(d) and ONIOM[CAS(10,7)/6-31G(d):RHF/6-31G(d)]	
	$S_{0,FC}$	
	MP2/6-31G(d)	ONIOM[CASSCF(10,7)/6-31G(d):RHF/6-31G(d)]
C_6N_2	1.46	1.45
N_8O_{11}	1.24	1.19
N_8N_3	1.41	1.36
C_1N_3	1.46	1.47
C_7N_3	1.46	1.45
$N_{19}O_{20}$	1.24	1.19
$N_{10}N_{19}$	1.41	1.36
C_6N_{10}	1.46	1.45
C_7N_{10}	1.46	1.45
	Bond Angles (deg)	
$O_{14}N_9O_{13}$	127.1	126.3
$O_{14}N_9N_2$	116.4	118.2
$C_1N_2N_9$	112.7	112.6
$C_6N_2N_9$	112.7	113.5
$O_{12}N_8O_{11}$	1.27.1	126.0
$O_{11}N_8N_3$	116.42	117.0
$C_1N_3N_8$	112.7	115.0
$O_{20}N_{19}O_{21}$	127.1	126.0
$O_{20}N_{19}N_{10}$	116.4	116.9
$C_6N_{10}N_{19}$	112.7	115.5
	Dihedral Angles (deg)	
$O_{13}N_9N_2C_6$	24.48	23.90
$O_{11}N_8N_3C_1$	24.49	18.00
$O_{20}N_{19}N_{10}C_6$	−24.49	−18.00

Search for critical points (minima, transition states, and CIs) on excited-electronic-state and ground-state PESs for RDX was performed at the ONIOM[CASSCF(10,7)/6-31G(d):UFF] level of theory with the Gaussian 09 program.[21a] No symmetry restrictions were applied during the calculations. An active space comprising 10 electrons in 7 orbitals, denoted as CASSCF(10,7), was used for the active site of RDX. The orbitals included one nonbonding $n\pi_O$, two nonbonding $n\sigma_O$, one bonding π_{ONO}, one antibonding π_{ONO}^*, one bonding σ_{NN}, and one antibonding σ_{NN}^*. This choice generated 10 electrons distributed among 7 active orbitals. Choice of one bonding σ_{NN}, one antibonding σ_{NN}^*, and nonbonding $n\sigma_O$ orbitals in the active space is justified by the fact that the part of the PESs of RDX explored here incorporates the nitro−nitrite isomerization reaction coordinate, which involves N−N bond elongation and O−N bond formation. Further discussion of the selection of a (10,7) active space for $N-NO_2$ systems in general can be found in our previous publications.[15] Vertical excitation energies were computed by state averaging over the ground state and two successive singlet excited states with equal weights. The initial two-layer molecular geometry of RDX was drawn using GaussView software, which automatically provided all of the MM parameters, including bond order and bond connectivity. Partial atomic charges were also calculated using the UFF=QEQ key word for MM. The procedure should include all parameters required to monitor the bond breaking and formation required for RDX excited- and ground-state chemistry.

Furthermore, both steric and electrostatic interactions between the high- and low-level regions of RDX are incorporated in the ONIOM methodology using the $(E_{real}^{Low} - E_{active\ site}^{Low})$ term in the ONIOM extrapolation scheme. In this report, the coupling arising from steric hindrance is referred to as a steric effect, and the coupling arising from electrostatic interaction is referred to as an inductive effect. To improve the description of the electrostatic interactions between the two regions in the ONIOM calculations further, however, one can use the electronic embedding option, which might not be necessary for a given system. Electronic embedding incorporates the partial charges of the low-level region into the high-level QM Hamiltonian of the active site. Active-site geometries were compared with and without electronic embedding at a few critical points along the RDX PESs; no significant change in active site geometry was observed with this calculational difference. Therefore, embedded charge was not utilized for the calculations reported in this work.

The geometries of the critical points were optimized with state averaging over the S_0 and S_1 states with equal weights. Transition state (TS) structures were characterized by analytical frequency calculations. Equilibrium geometry calculations weare conducted taking the total charge as neutral and the spin multiplicity as 1. Steepest-descent paths (minimum-energy paths) were calculated using an intrinsic reaction coordinate (IRC) algorithm implemented in Gaussian 09.[21a] The IRC calculation was performed using the initial force constant calculated at the same level of theory. The selections of the level of theory and the active space

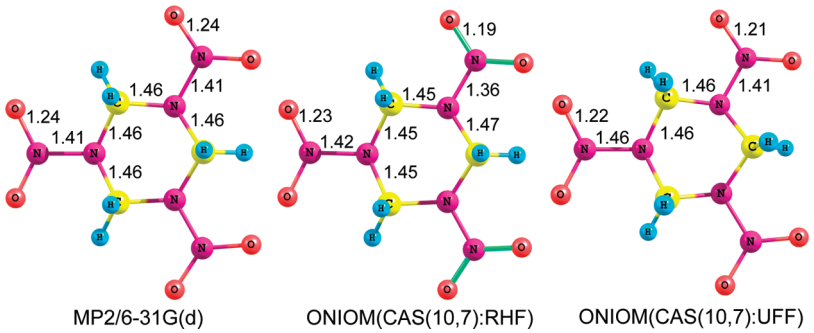

Figure 3. Equilibrium geometry of RDX computed at the MP2, ONIOM(CAS:RHF) (RHF = restricted Hartree−Fock), and ONIOM(CAS:UFF) levels of theory. The 6-31G(d) basis set was used for QM calculations, and a universal force field (UFF) was used for MM calculations. Respective bond lengths (Å) are indicated in the figure.

were justified by the comparison between the calculated vertical excitation energies and experimental absorption maxima presented in the Results section. A CASSCF(14,11) calculation gives similar results for RDX, but the smaller active space was chosen here to match the previous DMNA calculations.[15] Note that both inductive and steric effects are included in the ONIOM methodology. The HF approximation (QM method) employs spin orbitals, and therefore, it considers partial atomic charges in the molecule and polarizes the system automatically, modeling inductive effects. The MM method, on the other hand, calculates atomic charges using the UFF=QEQ keyword and thus models inductive effects directly. Additionally, selection of the active site at some constrained geometrical environment of the full molecule incorporates steric effects into the system.

III. RESULTS

IIIA. Equilibrium Geometries of RDX and DMNA. Ground-state optimization of RDX utilizing the two-layer ONIOM methodology described in the previous section was conducted by using the CASSCF method with a 6-31G(d) basis set for the high-level region and UFF for the low-level region. The optimized geometry ($S_{0,FC}$) of RDX is depicted in Figure 2, and important geometrical parameters related to this geometry are given in Table 1A. RDX can have a number of conformers. Here, only an EEE conformer, in which all NO_2 moieties are located in equatorial positions of the six-membered hydrotriazine ring of the molecule, is chosen as an example to illustrate that the ONIOM methodology can be successfully applied to explore the PESs of RDX. Other conformers are expected to behave similarly. Figure 3 and Table 1A show that bond angles, bond lengths, and the ONNC dihedral angles predicted for N−NO_2 moieties in the active site and in the remainder of the molecule for the EEE conformer, treated at different levels of theory, are similar and not significantly different.

In general, with a good combination of theory levels for the active site and the low-level region of the molecule for an ONIOM methodology, the predicted geometrical parameters should be (approximately) similar to those predicted by a pure quantum mechanical calculation. Therefore, a comparison of geometrical parameters of RDX predicted at the ONIOM(CAS:UFF) and MP2/6-31G(d) levels of theory was also performed to judge appropriateness of the CAS:UFF combination used in the present ONIOM methodology. Here, comparison of geometrical parameters of RDX predicted at the ONIOM(CAS:UFF) and pure QM CAS levels of theory was impossible to perform because the RDX molecule is too large to be treated with a pure CAS multiconfiguration SCF level of theory.

Table 2. Geometrical Parameters of DMNA at the CASSCF(10,7)/6-31G(d) Level

	FC/minimum/CI/TS		
	$S_{0,FC}$	$S_{1,Min}$	$(S_1/S_0)_{CI}$
	Bond Lengths (Å)		
N_2O_4	1.22	1.42	1.33
N_1N_2	1.46	1.45	2.83
N_2O_3	1.22	1.26	1.19
C_5N_1	1.45	1.46	1.44
C_6N_1	1.45	1.45	1.44
	Bond Angles (deg)		
$O_4N_2O_3$	126.4	110.4	111.8
$O_4N_2N_1$	116.8	108.1	54.5
$C_5N_1N_2$	111.7	109.9	112.8
$C_6N_1N_2$	111.7	107.9	113.4
	Dihedral Angles (deg)		
$O_4N_2N_1C_6$	−26.25	−153.2	−68.41
$O_3N_2N_1C_5$	26.25	−48.00	−45.62

The geometrical parameters for RDX computed at the MP2/6-31G(d) level of theory are given in Table 1B. The geometry is depicted in Figure 3. The agreement between the ONIOM(CAS:UFF) and MP2 results for the active site of RDX is excellent, in general. A minor difference between the ONIOM(CAS:UFF) and MP2 results, however, was found in the low-level region: For the low-level region of RDX, ONIOM(CAS:UFF) predicts the dihedral angle ONNC as ∼12°, whereas MP2 predicts the same dihedral angle as ∼25°. This small difference between the ONIOM(CAS:UFF) and MP2 results can be neglected.

Additionally, a (CAS:RHF) (RHF = restricted Hartree−Fock) combination wais also employed in another ONIOM method to judge whether the UFF MM provides a reasonable description of the structure of the low-level region of RDX. The geometrical parameters of RDX optimized at the ONIOM[CAS/6-31G(d):RHF/6-31G(d)] level of theory are given in Table 1B, and the corresponding optimized geometry is depicted in Figure 3. Table 1 clearly indicates that the ONIOM(CAS:RHF) methodology predicts a geometry for RDX similar to that rendered by the ONIOM(CAS:UFF) level of theory (see Figure 3). This

dx.doi.org/10.1021/jp109152p |J. Phys. Chem. A 2011, 115, 4135–4147

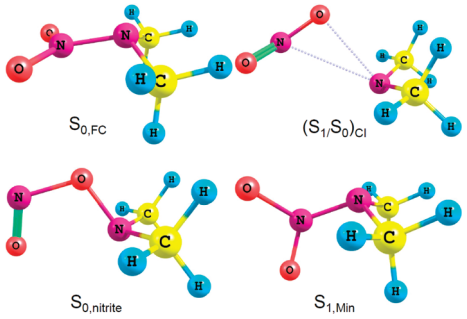

Figure 4. CASSCF(10,7)/6-31G(d)-optimized geometries of DMNA.

comparison of ONIOM(CAS:UFF) and ONIOM(CAS:RHF) suggests that UFF molecular mechanics is an adequate level of theory to predict the structure of the low-level region of RDX. Furthermore, the CAS:UFF combination in the ONIOM method saves considerable computational cost over the CAS:RHF combination. Therefore, in this work, a (CAS:UFF) combination was used in the ONIOM method to explore electronic PESs of RDX. Here, note that the above comparison among a pure QM method (MP2), a QM:MM combination in ONIOM [ONIOM(CAS:UFF)], and a QM:QM combination in ONIOM [ONIOM(CAS:RHF)] reveals the important fact that the ONIOM methodology breaks the symmetry of the RDX molecule, whereas MP2 retains the symmetry of the molecule.

The active site of RDX chosen for the ONIOM(CAS:UFF) calculation appears to resemble the structure of DMNA (see illustration in Figure 1). Based on this similarity, one can imagine that the electronic PESs of RDX might resemble those of DMNA; however, DMNA contains only a single $N-NO_2$ moiety that does not experience inductive and steric effects exerted by other $N-NO_2$ groups present in RDX. This difference might have significant effect on the relative topography of the PESs of these two molecules. To explore topographical differences of the PESs of these two molecules, the PESs of RDX and DMNA were compared. Geometrical parameters of DMNA optimized at a CASSCF(10,7)/6-31G(d) pure QM level of theory are given in Table 2, and its optimized geometry is illustrated in Figure 4. Tables 2 and 1A clearly indicate that the DMNA structure does represent the active-site structure of RDX: bond lengths, bond angles, and dihedral angles are all quite similar. Later in this report, however, we explain that this similarity is not maintained for the excited-electronic-state PESs of RDX and DMNA: critical points (such as CIs and transition states) for excited electronic states of DMNA are not similar to those for the active site of RDX, because of the influence of inductive and steric effects caused by the presence of other $N-NO_2$ moieties in the remainder of the RDX molecule.

IIIB. Electronic PESs of RDX and DMNA. RDX and DMNA, being members of the nitramine family, can potentially dissociate through a number of decomposition pathways, such as NO_2 elimination, HONO elimination, O elimination, and nitro−nitrite isomerization followed by NO elimination. Our previous nanosecond and femtosecond laser experiments, however, support only nitro−nitrite isomerization followed by NO elimination as the major decomposition pathway for electronically excited RDX and DMNA.[15,20] The experimental evidence for this conclusion is as follows: (1) NO rovibrational distributions indicate that NO_2 elimination is not a major decomposition channel; (2) no −N−NO fragment was observed in either femtosecond or nanosecond laser experiments, which excludes the role of O-elimination channel; (3) OH radical was not observed in LIF experiments, which excludes the possible role of an HONO elimination channel; and (4) observation of the $(CH_3)_2NOH$ radical by TOFMS directly indicates that a nitro−nitrite isomerization is involved in the overall exited-electronic-state decomposition of DMNA. Experimental results also suggest that RDX returns to the ground state following UV electronic excitation of the molecule and then dissociates to NO through a nitro−nitrite isomerization on its ground-state surface.[20] The primary reason for this conclusion is that the NO product is observed to be rotationally cold (20 K) but vibrationally hot (~1800 K). More details of these experimental results can be found in our previous publications.[15,20] Previous theoretical results,[15] on the other hand, suggest that DMNA dissociates on its S_1 excited state, generating rotationally hot (120 K) but vibrationally cold NO product. Furthermore, a number of CIs along the nitro−nitrite isomerization reaction coordinate are predicted to be involved in excited-electronic-state decomposition of DMNA. Similar involvement of CIs in the nitro−nitrite isomerization reaction coordinate was previously anticipated for excited-electronic-state decomposition of RDX;[15] however, direct theoretical evidence for this pathway is established for RDX in the present work.

As experimental results[20] suggest that the RDX molecule returns to the ground state following UV excitation to its low-lying excited electronic states, we provide here a complete decay path for this molecule from its low-lying excited electronic states to the ground state, explored at the ONIOM[CASSCF(10,7)/6-31G(d):UFF] level of theory. In this regard, a comparison between the computed vertical excitation energies and the experimentally obtained UV absorption maxima of RDX is first performed. The vertical excitation energies (E_{vert}) for RDX,

Table 3. RDX ONIOM-Calculated Excitation Energies of the Critical Points (FC Point, Minimum, Transition State) of RDX with Respect to the Energy of Its FC Geometry, Optimized at the ONIOM(CAS:UFF) and ONIOM(MP2:UFF) Levels of Theory

level	FC/min/TS/CI	ΔE (eV)
ONIOM[CASSCF(10,7)/6-31(d):UFF]	$S_{0,FC}$	0.00
	$S_{1,FC}$[a]	5.10
	$S_{2,FC}$[a]	5.88
	$S_{1,Min,Nitro}$	3.50
	$S_{1,Min,Nitrite}$	4.20
	$S_{1,TS,nitro-nitrite}$	5.50
	$S_{1,TS,NO-elimin}$	4.30
	$(S_2/S_1)_{CI}$	4.10
	$(S_1/S_0)_{CI}$	3.60
	$S_{0,Min,Nitrite}$	1.20
	$S_{0,TS,NO-elimin}$	1.50
ONIOM[MP2/6-31(d):UFF]	$S_{0,FC}$	0.00
	$N-NO_2$[b]	1.78
	$S_{0,TS,nitro-nitrite}$	4.00
	$S_{0,nitrite}$	0.98
	$S_{0,TS,NO-elimin}$	1.35

[a] Experimental UV spectrum of RDX in acetonitrile has two distinct maxima at 5.25 and 6.34 eV, the latter being most intense. [b] $N-NO_2$ bond dissociation energy of RDX previously calculated to be 1.69 eV at the B3LYP/6-31G(d) level of theory by Chakraborty et al.[24]

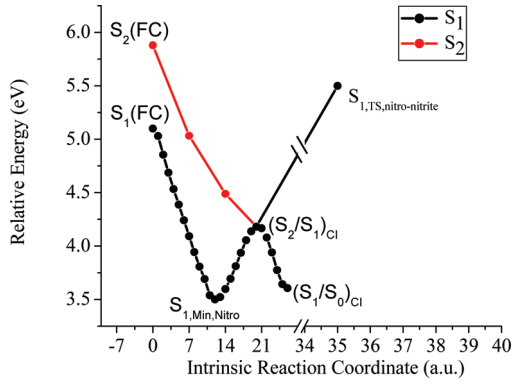

Figure 5. ONIOM(CASSCF:UFF) energy profile along the minimum-energy path on the S_2 and S_1 surfaces. The reaction coordinates for the two states (S_1 and S_2) are different.

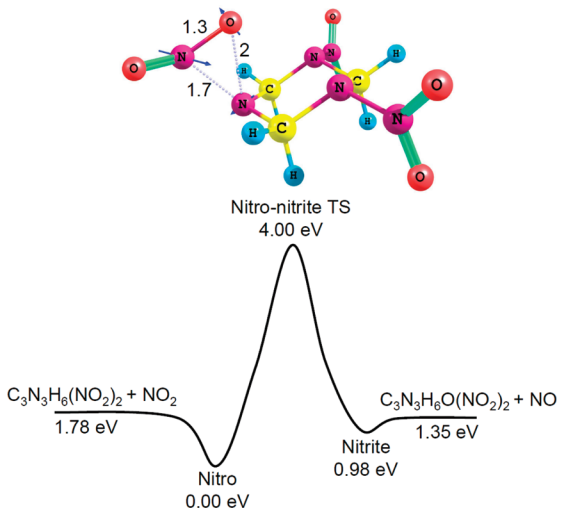

Figure 6. Ground-state PES of RDX for the nitro−nitrite isomerization channel and the N−NO_2 bond dissociation channel explored at ONIOM[MP2/6-31G(d):UFF]. Blue arrows indicate the unstable normal mode of vibration associated with the respective transition state.

computed at the ONIOM[CASSCF(10,7)/6-31G(d):UFF]-optimized Franck−Condon (FC) geometry (FC geometry at ground-state minimum) of C_1 symmetry, are listed in Table 3. The calculations show that the two lowest-lying excited electronic states (S_1 and S_2) for RDX have vertical excitation energies of 5.1 and 5.88 eV, respectively, and that both of them are of (n,π^*) character. The calculated vertical excitation energies of the S_1 and S_2 states of RDX are in reasonably good agreement with the experimental absorption maxima of 5.25 and 6.34 eV.[22] The disagreement between experiment and theory is around 0.5 eV for the S_2 state of RDX for the present ONIOM calculation; this falls into the commonly acceptable uncertainty range of ±0.5 eV for such calculations.[15a] Because the calculated excitation energies are compared to the acetonitrile solution-phase absorption data, a good part of this ±0.5 eV "accuracy range" can be associated with solvent and intermolecular effects that are present in acetonitrile polar solvent.

Furthermore, the vertical excitation energy of the S_1 state of RDX, computed at the ONIOM[CASSCF(10,7)/6-311+G(d):UFF] level of theory is 5.04 eV. {Note that ONIOM[CAS/6-31G(d):UFF] predicts 5.1 eV.} This indicates that addition of diffuse functions to the basis set or enlargement of the basis set does not improve the relative excitation energy significantly in the present calculation; however, computational time becomes considerably greater with enlarged basis sets. Inclusion of diffuse functions into the basis set can contribute to the behavior of ionic/charge-transfer or Rydberg states; however, it should not affect valence excited states, as appears to be the case here. This trend is evident not only in our CAS calculation, but also in CAS calculations performed by other groups:[23] if a balanced active space is provided in a CAS calculation, enlarging the basis set does not significantly improve relative excitation energies of the critical points. Therefore, in the present work, a 6-31G(d) basis set is used for all calculations to maintain optimum conditions for computational cost and accuracy.

Comparison of the experimental excitation energies (5.5 eV at 226 nm, 5.26 eV at 236 nm, 5.00 eV at 248 nm, and 4.8 eV at 258 nm) used in previous photofragmentation-fragment detection experimental work[20] with the calculated vertical excitation energies at the ONIOM[CASSCF(10,7)/6-31G(d):UFF] level indicates that these UV photoexcitations of RDX primarily populate lower vibrational manifolds of the S_2 surface or upper vibrational manifolds of the S_1 surface.

A number of critical points on electronically excited-state PESs of RDX such as $(S_2/S_1)_{CI}$, $(S_1/S_0)_{CI}$, $S_{1,TS}$ associated with nitro−nitrite isomerization, and $S_{1,Min}$ were optimized using Gaussian 09.[21] Optimized geometries are shown in Figure 2 with important bond lengths. The minimum-energy pathways connecting different critical points to the respective FC points of the S_1 and S_2 states were also explicitly calculated at the ONIOM-(CAS:UFF) level and are depicted in Figure 5. The decay paths connecting the FC point of the S_2 state to $(S_2/S_1)_{CI}$ on the S_2 surface and $(S_2/S_1)_{CI}$ to $(S_1/S_0)_{CI}$ on the S_1 surface were calculated to be barrierless. Figure 5 also shows the decay path from the FC point of the S_1 state to the minimum of the S_1 state $(S_{1,Min,Nitro})$ and an energy profile for nitro−nitrite isomerization on the S_1 surface. The isomerization path on the S_1 surface has an activation barrier of 2 eV (46 kcal/mol) with respect to $S_{1,Min,Nitro}$. Therefore, upon electronic excitation of RDX to or near the FC point to the S_2 state, the molecule should follow a barrierless steepest-descent pathway connecting the FC point of S_2 state to $(S_2/S_1)_{CI}$ and then from $(S_2/S_1)_{CI}$ to $(S_1/S_0)_{CI}$. This pathway should finally lead the molecule to its ground state. The nitro−nitrite isomerization path on the S_1 surface is not energetically favorable, as it has an activation barrier of ~2 eV with respect to the S_1 minimum.

After the molecule comes back to the ground state through $(S_1/S_0)_{CI}$, a number of fragmentation channels can open for RDX. To understand these different possible channels on the ground-state PES of RDX, different critical points and related minimum-energy paths on the S_0 state of RDX were explored. Undoubtedly, the steepest-descent path from $(S_1/S_0)_{CI}$ would be the primary decomposition channel for this molecule.[21b] A key feature of crossing geometries is that more than one relaxation direction might exist; nonetheless, the steepest path that coincides with the initial momentum is usually the favored one. Before addressing the steepest-descent path connecting $(S_1/S_0)_{CI}$ on the ground state, we first point out a number of important insights on ground-state decomposition of RDX explored at the ONIOM(MP2:UFF) level of theory. Later, exploration of the ground-state PES of RDX at the ONIOM-(CAS:UFF) level of theory is described.

Nitro−nitrite isomerization of RDX followed by NO elimination or NO_2 elimination on its S_0 surface can easily be explored at

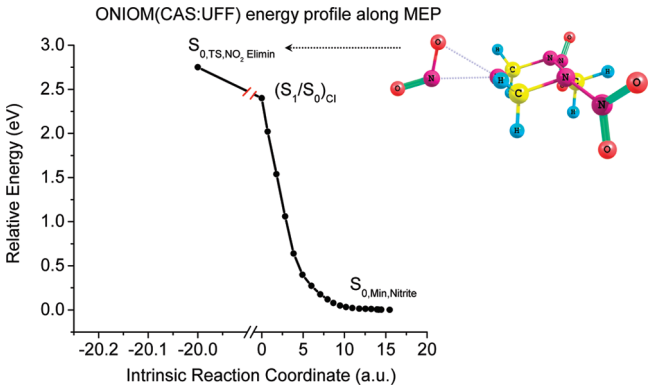

Figure 7. ONIOM(CASSCF:UFF) energy profile of RDX along the minimum-energy path on the S_0 surface.

the ONIOM(MP2/6-31G(d):UFF) level of theory. A tight (with a short N−N bond distance in the N−NO_2 active site) nitro−nitrite TS was localized on the ground-electronic-state surface of RDX, as shown in Figure 6. The N−N bond distance was predicted to be 1.7 Å, and the N−O bond distance was predicted to be 2.0 Å (see Figure 6) in the active site of RDX. The activation energy associated with nitro−nitrite isomerization of RDX at the ONIOM(MP2:UFF) level was calculated to be 4 eV. The ONIOM(MP2:UFF) level of theory predicts activation energies for the NO elimination TS following nitro−nitrite isomerization and N−NO_2 bond dissociation energy barrier from RDX of 1.35 and 1.78 eV, respectively. The N−NO_2 bond dissociation energy barrier of 1.78 eV for RDX predicted by ONIOM(MP2:UFF) is in good agreement with a previous computational result of 1.69 eV obtained with a B3LYP pure QM method by Chakraborty et al.[24] This comparison suggests that use of the UFF MM method for the low-level region of RDX does not significantly affect calculated activation energies for reactions that occur at the active site (one N−NO_2 moiety) of the molecule.

Therefore, these results indicate that, if the RDX molecule is thermally dissociated on the ground-state surface only, the major decomposition channel should be N−NO_2 bond dissociation because this channel is associated with the lowest activation barrier. If the molecule evolves from the upper excited state (S_1) to the ground state, however, $(S_1/S_0)_{CI}$ becomes important, and the steepest-descent path on the ground state connecting $(S_1/S_0)_{CI}$ becomes primary decomposition pathway. The minimum-energy pathway associated with internal conversion of the molecule from the upper excited state (S_1) to the ground state was explored at ONIOM[CAS(10,7)/6-31G(d):UFF] level of theory and is addressed below.

The ONIOM[CASSCF(10,7)/6-31G(d):UFF] level of theory could not predict a tight nitro−nitrite isomerization TS as predicted by ONIOM(MP2:UFF) discussed above. Instead, ONIOM(CAS:UFF) predicted an $(S_1/S_0)_{CI}$ conical intersection, which was calculated to be 3.6 eV higher in energy than the ground-state minimum of RDX. The smallest adiabatic energy gap between the S_0 and S_1 surfaces near the $(S_1/S_0)_{CI}$ CI of RDX was computed to be 16 cm^{-1}, which suggests that the S_1 and S_0 surfaces are strongly nonadiabatically coupled with each other.[26] Therefore, these results suggest that, when electronic nonadiabatic effects are present, a multiconfiguration-based methodology becomes absolutely necessary to describe even the ground-state PES. In the present case, the ground-state PES of RDX predicted by ONIOM(MP2:UFF) along the nitro−nitrite isomerization reaction coordinate was nothing but an artifact of the single-configuration methodology.

Figure 7 shows the minimum-energy decay paths from $(S_1/S_0)_{CI}$ to nitrite ($S_{0,Min,Nitrite}$) and an energy profile connecting the transition state for NO_2 elimination ($S_{0,TS,NO2\text{-}elimin}$) from nitrite and $(S_1/S_0)_{CI}$. Paths were explicitly calculated using the intrinsic reaction coordinate (IRC) algorithm. Figure 7 directly indicates that, if the RDX molecule comes back to the ground state following $(S_1/S_0)_{CI}$ CI, the steepest-descent path is associated with nitro−nitrite isomerization. The NO_2 elimination pathway on the S_0 state following $(S_1/S_0)_{CI}$ incorporates an activation barrier of 0.35 eV, which makes this channel energetically unfavorable.

To summarize the above results, a schematic one-dimensional plot of the multidimensional singlet PESs (S_0, S_1, and S_2) of RDX along the minimum-energy (steepest-descent) paths with locations and structures of different critical points and CIs is presented in Figure 8. This schematic one-dimensional plot of the PESs of RDX was drawn from Figures 7 and 5 to provide a concise description of all nonadiabatically coupled electronic PESs of RDX together. Figure 8 shows that, following vertical excitation of RDX to its even lower vibronic manifold of the S_2 surface at or near 226 nm (5.5 eV), the molecule can undergo rapid nonadiabatic internal conversion from S_2 to S_1 through $(S_2/S_1)_{CI}$ and, thereafter, from S_1 to S_0 through $(S_1/S_0)_{CI}$. Thus, in this pathway, the molecule stores electronic excitation energy into its vibrational degrees of freedom on the ground-state surface. To undergo NO_2 elimination from $(S_1/S_0)_{CI}$ on the ground state, the RDX molecule has to surmount an activation barrier of 8 kcal/mol; however, the nitrite formation pathway from $(S_1/S_0)_{CI}$ is barrierless. The reaction coordinates of the minimum-energy decay paths depicted in Figure 8 are composed of changes in the N−N bond length, ONN bond angles, and ONNC dihedral angles of the active site of RDX. The structural changes indicate that an isomerization occurs from nitro to nitrite for RDX as the molecule is relaxing back to its ground state from the FC point of the S_2 surface. Figure 8 also clearly indicates that the nitro−nitrite isomerization process is electronically nonadiabatic in nature because of the involvement of a number of conical intersections.

The structure of RDX at $(S_2/S_1)_{CI}$ presents an N−NO_2 bond distance of 2.21 Å (see Table 1A and Figure 2) for the active site of RDX. The structure of $(S_1/S_0)_{CI}$ shows a nitro−nitrite isomerization transition-state geometry that has an O−N distance of 2.4 Å and an N−N bond distance of 2.9 Å for the active site of the molecule. The geometry at $(S_1/S_0)_{CI}$ gives a loose nitro−nitrite transition-state geometry for which the NO_2 moiety in the active site of RDX interacts with the rest of the molecule from a long distance (~2.9 Å). The molecule isomerizes to a nitrite form on its S_0 surface and undergoes NO elimination, surmounting a negligible energy barrier (~0.3 eV; see Figure 8), to the NO elimination transition state. The force components on N and O atoms for the unstable normal mode of vibration for the NO-elimination TS on the S_0 surface of RDX are parallel; this TS is thereby predicted to produce little torque on the terminal NO moiety. Therefore, decomposition of the RDX molecule, following nonadiabatic relaxation through first $(S_2/S_0)_{CI}$ and then $(S_1/S_0)_{CI}$ followed by NO elimination on the ground-state surface, is expected to produce a rotationally cold NO product. Determination of the exact rotational temperature of the NO product requires determination of the internal-state population of

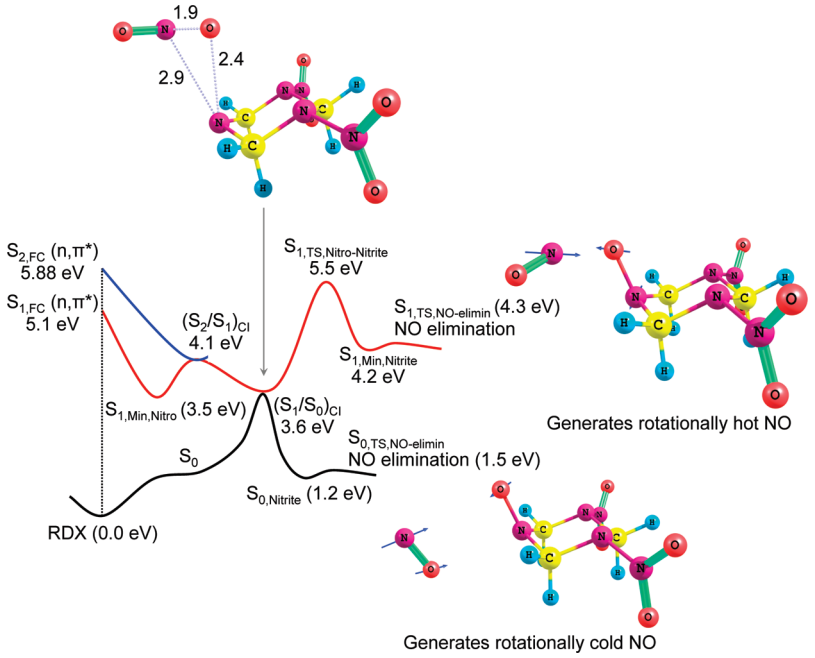

Figure 8. Schematic one-dimensional plot of the multidimensional electronic potential energy surfaces of RDX computed at the ONIOM[CASSCF-(10,7)/6-31G(d):UFF] level of theory. Blue arrows indicate the unstable normal mode of vibration associated with the respective transition state. Following electronic excitation to the S_2 state, the molecule follows the minimum-energy path: S_2(FC) → (S_2/S_1)CI → $(S_1/S_0)_{CI}$ → S_0(nitrite) → NO elimination.

the NO products using statistical theories, which is beyond the scope of the present study.

Another possible energetically unfavorable decomposition pathway of RDX from the FC point of the S_2 surface would be initial nonadiabatic deactivation of the molecule to the S_1 surface through the $(S_2/S_1)_{CI}$ CI. After the molecule has crossed the $(S_2/S_1)_{CI}$ CI, nitro−nitrite isomerization can be initiated on the S_1 surface. This process, however, requires an activation energy barrier of 2 eV to be surmounted on the S_1 surface of RDX (see Figure 8) with respect to $S_{1,Min,Nitro}$. Subsequent nitrite formation and NO elimination on the S_1 surface are almost barrierless. The unstable normal mode of vibration for the NO elimination transition state on the S_1 surface of RDX clearly shows a large component of force on the N atom only. This force imbalance is expected to produce considerable torque on the terminal NO moiety. Therefore, decomposition of the molecule through nitro−nitrite isomerization followed by NO elimination on the S_1 surface is expected to produce a rotationally hot NO product. To proceed through this pathway, however, RDX first has to surmount a high activation barrier of 2 eV on the S_1 surface. Such a high activation barrier on the S_1 surface makes this process less probable with regard to the aforementioned process involving the S_0 surface for decomposition of excited-electronic-state RDX.

A comparison of DMNA excited-state PESs, predicted at a pure CASSCF QM method, and RDX excited-state PESs, predicted with the ONIOM(CAS:UFF) methodology, was also conducted to assess the influence of the steric and inductive effects generated by other N−NO_2 groups on the excited-state PESs created for the active site of RDX in the ONIOM methodology. The vertical excitation energies (E_{vert}) for DMNA, calculated at their CASSCF(10,7)/6-31G(d)-optimized FC geometry, are listed in Table 4. The calculated vertical excitation energies of the S_2 and S_3 states are 5.65 and 6.6 eV (see Table 4), respectively, which are in good agreement with the experimental

Table 4. DMNA CASSCF(10,7)/6-31G(d)-Calculated Vertical Excitation Energies and Relative Energies of the CIs with Respect to the Energy of the FC Geometry, Optimized at the Same Level of Theory[15b]

state/CI	Δ*E* (eV)
S_1 (FC)	4.83
S_2 (FC)	5.65
S_3(FC)	6.6
$(S_1/S_0)_{CI}$	2.6
$(S_2/S_1)_X$[a]	4.8
$(S_2/S_1)_{CI}$	4.2

[a] Two S_2/S_1 CIs are localized on the S_2 surface, one at shorter N−N bond distance defined as $(S_2/S_1)_X$ and another at longer N−N bond distance defined as $(S_2/S_1)_{CI}$. See text for more detail.

values of 5.39 and 6.42 eV.[25] Therefore, CASSCF computation indicates that DMNA is excited to its S_2 (n,π^*) state with a 226-nm excitation wavelength, as was used in our previous experiments.[15b]

A schematic one-dimensional plot of the multidimensional singlet PESs (S_0, S_1, and S_2) of DMNA with locations and structures of different critical points is plotted in Figure 9. Three CIs between singlet surfaces can be localized for DMNA: (1) $(S_1/S_0)_{CI}$, CI between S_1 and S_0 surfaces; (2) $(S_2/S_1)_X$, CI between S_2 and S_1 surfaces at short N−N bond distance; and (3) $(S_2/S_1)_{CI}$ CI between S_2 and S_1 surfaces at long N−N bond distance. The structure of DMNA at both $(S_1/S_0)_{CI}$ and $(S_2/S_1)_{CI}$ represents a loose geometry in which the NO_2 moiety interacts with the $(CH_3)_2N$ moiety from a long distance (∼2.8 Å). The relative CASSCF energies of the CIs on both excited and ground singlet PESs of DMNA with respect to the energy of the ground-state FC geometry are listed in Table 4.

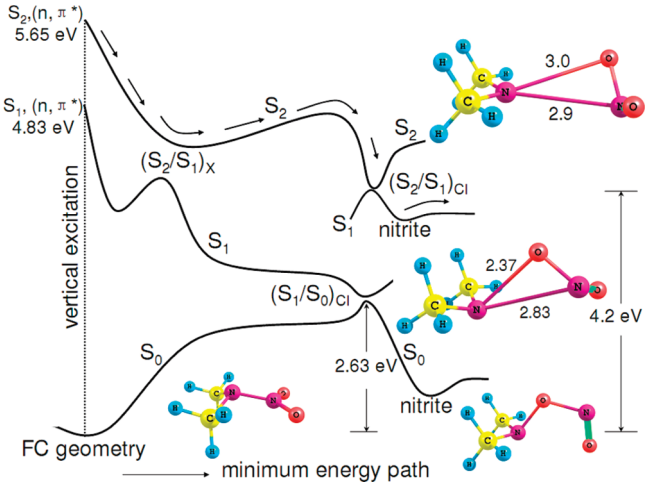

Figure 9. Schematic one-dimensional plot of multidimensional electronic potential energy surfaces of DMNA computed at the CASSCF(10,7)/6-31G(d) level of theory. Note that the $(S_2/S_1)_X$ conical intersection is weakly nonadiabatically coupled and that the adiabatic energy gap near this conical intersection was computed to be 485 cm^{-1}. $(S_2/S_1)_{CI}$ and $(S_1/S_0)_{CI}$ are strongly nonadiabatically coupled conical intersections. Arrows indicate the nonadiabatic minimum-energy path of DMNA following electronic excitation of the molecule to the FC point of the $S_2(n,\pi^*)$ state.

On the basis of the results presented above, one finds that vertical excitation to the FC point in the S_2 state can potentially lead DMNA to a nonadiabatic nitro−nitrite isomerization through the $(S_2/S_1)_{CI}$ CI. This CI is energetically accessible from the FC point of the S_2 surface, because this point is lower in energy than the vertical excitation to the S_2 surface. After crossing the $(S_2/S_1)_{CI}$ CI, DMNA can be directed to the isomerization product on the S_1 surface. Another possible decomposition pathway from the FC point of the S_2 surface would be nonadiabatic deactivation of the molecule to the S_1 surface through the $(S_2/S_1)_X$ CI. After crossing the $(S_2/S_1)_X$ CI, DMNA can be directed to another surface crossing, the $(S_1/S_0)_{CI}$ CI. This will finally lead the system to the nitro−nitrite isomerization on the S_0 surface. The dominant process, however, depends on the strength of nonadiabatic coupling between adiabatic surfaces near CIs.[26]

A small energy gap between adiabatic surfaces enhances the probability of nonadiabatic transition from the upper electronic state to the lower electronic state near the CI. The computed energy gaps between the S_2 and S_1 adiabatic surfaces near $(S_2/S_1)_X$ and $(S_2/S_1)_{CI}$ are 487 and 0.73 cm^{-1}, respectively, at the CASSCF(10,7)/6-31G(d) level of theory. Therefore, the nonadiabatic transition through $(S_2/S_1)_{CI}$ will dominate that through $(S_2/S_1)_X$. As a result, nitro−nitrite isomerization through the $(S_2/S_1)_{CI}$ CI on the S_1 surface is expected to be the major decomposition channel of DMNA from the FC point of the S_2 surface. Furthermore, the CASSCF level of theory also predicts that, on the S_1 surface, the nitrite form of DMNA dissociates into the NO product through the NO-elimination transition state (S_1/TS). The unstable normal mode of vibration for the S_1/TS transition state shows torque acting on the NO moiety. Therefore, this nonadiabatic nitro−nitrite isomerization pathway followed by the NO elimination on the S_1 surface is predicted to yield rotationally hot NO products, in agreement with the experimental results.[15] Note too that the S_1 PES dissociation of DMNA should yield a cold vibrational distribution for NO because the molecular internal energy of DMNA is partially sequestered in the electronic excitation of DMNA.

The PESs of RDX presented above were calculated assuming that electronic excitation was entirely localized in one N−NO_2 group (the active site). With regard to only this assumption, the PESs of RDX are expected to resemble those of DMNA. Nonetheless, as can be seen in Figures 8 and 9, the excited-state PESs of RDX do not resemble those of DMNA. This difference between RDX and DMNA is certainly related to steric and inductive effects (through electrostatic and other interactions) of the other N−NO_2 groups present in RDX but absent in DMNA. Therefore, DMNA is not a good model for RDX with regard to behavior of these two molecules following electronic excitation. Furthermore, when an ONIOM(CAS:UFF) calculation is performed for RDX, the molecule is broken into two parts: the active site and the remainder of the molecule. The active site of the molecule $[(CH_2)_2NNO_2]$ is treated at a CAS level of theory by replacing a C−C bond by a C−H bond in the RDX molecule, which finally results in a DMNA geometry $(CH_3)_2NNO_2$. The orbitals chosen for the active sites of RDX and DMNA were the same. Therefore, the difference in excited-electronic-state decomposition of RDX and DMNA did not result from orbitals chosen for the active spaces of these two systems.

IV. DISCUSSION AND CONCLUSIONS

In the present study, decomposition of isolated, excited-electronic-state RDX was investigated utilizing the ONIOM methodology. CASSCF was employed as the high-level method for the selected active site (one N−NO_2 moiety for RDX), and UFF was used as the low-level method for the remainder of the molecule. Rotationally cold NO product was predicted to be a major decomposition product of RDX following its electronic excitation. This prediction is consistent with previous experimental observations.[20] The NO product is generated through nitro−nitrite isomerization. The present ONIOM(CAS:UFF) level of theory predicts the following pathway for RDX decomposition from its S_2 excited state:

$$\mathrm{RDX\ (nitro, S_0, FC)} + h\nu\ (\sim 5.5 - 4.8\ \mathrm{eV}) \rightarrow$$

$$\mathrm{RDX^*\ (nitro, S_2)} \rightarrow (S_2/S_1)_{CI} \rightarrow (S_1/S_0)_{CI} \rightarrow$$

$$\mathrm{nitrite\ (S_0)} \rightarrow \mathrm{NO\ (rotationally\ cold,\ vibrationally\ hot)}$$

Our previous laser-induced fluorescence (LIF) experiments[15b] indicated that electronic excitation of RDX at 226 nm does not populate the S_1 minimum. Instead, RDX undergoes ultrafast (<180 fs) internal conversion to the ground state and then dissociates. In the present work, we did not test[27] theoretically why population does not end up in the S_1 minimum; rather, here, we explored the paths that can model our previous experimental observations. This pathway produces a rotationally cold but vibrationally hot distribution for the NO product from excited-electronic-state decomposition of RDX. The above decomposition pathway for RDX is predicted to be barrierless because of the presence of $(S_2/S_1)_{CI}$ and $(S_1/S_0)_{CI}$ CIs. Moreover, this barrierless pathway is suggestive of the experimental observation that the dynamics of the decomposition of RDX at 226 nm (equivalent to electronic excitation to the S_2 state) is faster than 180 fs.[20c] Only a few vibrations of the electronically excited gas-phase RDX molecule lead to molecular dissociation on this ultrafast time scale. The present theoretical calculations using the ONIOM methodology also predict that decomposition of

RDX occurs on the S_0 PES with high vibrational excitation after nonadiabatic evolution of the molecule through a series of CIs from the S_2 excited state. This prediction corroborates the experimental observation of vibrationally hot (1800 K) NO products. The above comparison of theoretical predictions and previous experimental observations suggests that, when the ONIOM methodology is suitably combined with the CASSCF algorithm, it can reliably explore hitherto-unknown excited-electronic-state PESs of energetic nitramine materials such as RDX, HMX, and CL-20.

Pure QM CASSCF calculations for DMNA, a simple analogue molecule of energetic nitramine materials with a single $N-NO_2$ moiety, on the other hand, show that for similarly excited DMNA, decomposition occurs on the S_1 surface. The following pathway is predicted at the CASSCF(10,7)/6-31G(d) level of theory:

$$\text{DMNA (nitro, } S_0\text{, FC)} + h\nu\ (\sim 5.5\ \text{eV}) \rightarrow$$

$$\text{DMNA}^{*}\ \text{(nitro, } S_2) \rightarrow (S_2/S_1)_{CI} \rightarrow \text{nitrite } (S_1) \rightarrow$$

$$\text{NO (rotationally hot, vibrationally cold)}$$

This pathway produces rotationally hot (120 K) but vibrationally cold [with only the (0−0) transition of NO observed experimentally] distributions for the NO product. Comparison of the decompositions of excited-electronic-state DMNA and RDX implies that the influence of other $N-NO_2$ moieties located at alternating positions about the six-membered ring of RDX is an important component for true energetic system behavior. Following electronic excitation of RDX and DMNA, RDX relaxes back to its S_0 PES, producing rotationally cold but vibrationally hot NO product; on the other hand, DMNA relaxes back to its S_1 PES, generating rotationally hot but vibrationally cold NO product.

Thus, the above discussion suggests that the specific topography of excited-electronic-state PESs of RDX, a true energetic system, allows this molecule to undergo ultrafast internal conversion to the ground-state surface through an electronically nonadiabatic, barrierless relaxation pathway. This pathway finally results in generation of rotationally cold and vibrationally hot products. The topography of the excited-electronic-state PESs of DMNA, a model nitramine system, on the other hand, does not provide a barrierless relaxation pathway to its ground electronic state. In this case, DMNA dissociates on its excited-state PES. This topographical difference between the excited-state PESs of RDX and DMNA might be the essential issue that controls the energetic behavior of energetic nitramine molecules, and it arises because of both steric and inductive effects on the $N-NO_2$ active site present in the RDX molecule. Both of these effects are incorporated into calculations using the ONIOM methodology.

The present work is significant for a number of reasons. First, electronic excited-state PESs of large energetic nitramine materials such as RDX have not been previously explored. The present effort employing the ONIOM/CASSCF methodology not only provides a number of detailed insights into the topography of the excited-state PESs of RDX, but also shows a possible way to calculate excited-electronic-state PESs of even larger energetic materials, such as CL-20 and PETN (pentaerythritol tetranitrate). Second, to date, only a single study[19] predicting potential application of the ONIOM methodology coupled with CASSCF to explore nonadiabatic processes of large molecules through CIs has been reported in the literature. Third, the present work successfully shows that the ONIOM methodology, coupled with a CASSCF algorithm, can predict nonadiabatic processes for large energetic molecules such as RDX: theoretical prediction fully corroborates experimental findings. The only significant assumption made for the ONIOM methodology is that electronic excitation is localized on one of the $N-NO_2$ moieties (considered the active site in the ONIOM calculation) of the RDX molecule.

AUTHOR INFORMATION

Corresponding Author

*E-mail: erb@lamar.colostate.edu.

Present Addresses

[†]Chemistry Department, Brookhaven National Laboratory, Upton, NY 11973.

ACKNOWLEDGMENT

These studies were supported by a grant from the U.S. Army Research Office (ARO).

REFERENCES

(1) Bernstein, E. R. In *Overviews of Recent Research on Energetic Materials*; Shaw, R., Brill, T., Thompson, D., Eds.; World Scientific: Singapore, 2004; pp 161−190

(2) Williams, F. E. *Adv. Chem. Phys.* **1971**, *21*, 289.

(3) Sharma, J.; Beard, B. C.; Chaykovsky, M. *J. Phys. Chem.* **1991**, *95*, 1209.

(4) Gilman, J. *J. Philos. Mag. B* **1995**, *71*, 1057.

(5) Kuklja, M. M.; Aduev, B. P.; Aluker, E. D.; Krasheninin, V. I.; Krechetov, A. G.; Mitrofanov, A. Y. *J. Appl. Phys.* **2001**, *89*, 4156.

(6) Windawi, H. M.; Varma, S. P.; Cooper, C. B.; Williams, F. *J. Appl. Phys.* **1976**, *47*, 3418.

(7) Schanda, J.; Baron, B.; Williams, F. *Acta Techn. Acad. Sci. Hung.* **1975**, *80*, 185.

(8) Schanda, J.; Baron, B.; Williams, F. *J. Lumin.* **1974**, *9*, 338.

(9) Varma, S. P.; Williams, F. *J. Chem. Phys.* **1973**, *59*, 912.

(10) Hall, R. B.; Williams, F. *J. Chem. Phys.* **1973**, *58*, 1036.

(11) Williams, F. *Advanced Chem. Phys.* **1971**, *21*, 289.

(12) Dremin, A. N.; Klimenko, V. Y.; Davidoua, O. N.; Zolodeva, T. A. In *Proceedings of the 9th Symposium (International) on Detonation*; Morat, W. J., Ed.; OCNR 113291-7; Office of Naval Research: Arlington, VA, 1989; p 319.

(13) Sharma, J.; Forbes, J. W.; Coffey, C. S.; Liddiard, T. P. *J. Phys. Chem.* **1987**, *91*, 5139.

(14) Sharma, J. Presented at the *APS Topical Meeting on Shocks in Energetic Materials*, Williamsburg, VA, 1991.

(15) (a) Bhattacharya, A; Guo, Y. Q.; Bernstein, E. R. *Acc. Chem. Res.* **2010**, *43*, 1476. (b) Bhattacharya, A.; Guo, Y. Q.; Bernstein, E. R. *J. Phys. Chem. A* **2009**, *113*, 811.

(16) Bearpark, M. J.; Ogliaro, F.; Vreven, T.; Boggio-Pasqua, M.; Frisch, M. J.; Larkin, S. M.; Robb, M. A. *J. Photochem. Photobiol. A* **2007**, *190*, 207.

(17) (a) Svensson, M.; Humbel, S.; Froese, R. D. J.; Matsubara, T.; Sieber, S.; Morokuma, K. *J. Phys. Chem.* **1996**, *100*, 19357. (b) Svensson, M.; Humbel, S.; Morokuma, K. *J. Chem. Phys.* **1996**, *105*, 3654. (c) Humbel, S.; Sieber, S.; Morokuma, K. *J. Chem. Phys.* **1996**, *105*, 1959. (d) Vreven, T.; Morokuma, K. *J. Comput. Chem.* **2000**, *21*, 1419. (e) Morokuma, K. *Philos. Trans. R. Soc. London, Ser. A* **2002**, *360*, 1149. (f) Vreven, T.; Morokuma, K. In *Annual Reports in Computational Chemistry*; Spellmeyer, D., Ed.; Elsevier: New York, 2010; Vol. 2, pp 35−52.

(18) (a) Blomgren, F.; Larsson, S. *J. Phys. Chem. B* **2005**, *109*, 9104. (b) Yamada, A.; Ishikura, T.; Yamato, T. *Protein: Struct, Funct, Bioinf.*

2004, *55*, 1063. (c) Gascon, J. A.; Batista, V. S. *Biophys. J.* **2004**, *87*, 2931. (d) Raynaud, C.; Poteau, R.; Maron, L.; Jolibois, F. *J. Mol. Struct. (THEOCHEM)* **2006**, *771*, 43. (e) Casadesus, R.; Moreno, M.; Lluch, J. M. *J. Photochem. Photobiol. A* **2005**, *173*, 365. (f) Zhang, R. B.; Ai, X. C.; Zhang, X. K.; Zhang, Q. Y. *J. Mol. Struct. (THEOCHEM)* **2004**, *680*, 21. (g) Walch, S. P. *Chem. Phys. Lett.* **2003**, *374*, 501. (h) Vreven, T.; Morokuma, K. *J. Chem. Phys.* **2000**, *113*, 2969. (i) Vreven, T.; Morokuma, K. *Theor. Chem. Acc.* **2003**, *109*, 125.

(19) Bearpark, M. J.; Larkin, S. M.; Vreven, T. *J. Phys. Chem. A* **2008**, *112*, 7286.

(20) (a) Im, H.-S.; Bernstein, E. R. *J. Chem. Phys.* **2000**, *113*, 7911. (b) Guo, Y. Q.; Greenfield, M.; Bernstein, E. R. *J. Chem. Phys.* **2005**, *122*, 244310. (c) Greenfield, M; Guo, Y. Q.; Bernstein, E. R. *Chem. Phys. Lett.* **2006**, *430*, 277. (d) Guo, Y. Q.; Greenfield, M.; Bhattacharya, A.; Bernstein, E. R. *J. Chem. Phys.* **2007**, *127*, 154301.

(21) (a) Frisch, M. J.; Trucks, G. W.; Schlegel, H. B.; Scuseria, G. E.; Robb, M. A.; Cheeseman, J. R.; Scalmani, G.; Barone, V.; Mennucci, B.; Petersson, G. A.; Nakatsuji, H.; Caricato, M.; Li, X.; Hratchian, H. P.; Izmaylov, A. F.; Bloino, J.; Zheng, G.; Sonnenberg, J. L.; Hada, M.; Ehara, M.; Toyota, K.; Fukuda, R.; Hasegawa, J.; Ishida, M.; Nakajima, T.; Honda, Y.; Kitao, O.; Nakai, H.; Vreven, T.; Montgomery, J. A., Jr.; Peralta, J. E.; Ogliaro, F.; Bearpark, M.; Heyd, J. J.; Brothers, E.; Kudin, K. N.; Staroverov, V. N.; Kobayashi, R.; Normand, J.; Raghavachari, K.; Rendell, A.; Burant, J. C.; Iyengar, S. S.; Tomasi, J.; Cossi, M.; Rega, N.; Millam, N. J.; Klene, M.; Knox, J. E.; Cross, J. B.; Bakken, V.; Adamo, C.; Jaramillo, J.; Gomperts, R.; Stratmann, R. E.; Yazyev, O.; Austin, A. J.; Cammi, R.; Pomelli, C.; Ochterski, J. W.; Martin, R. L.; Morokuma, K.; Zakrzewski, V. G.; Voth, G. A.; Salvador, P.; Dannenberg, J. J.; Dapprich, S.; Daniels, A. D.; Farkas, Ö.; Foresman, J. B.; Ortiz, J. V.; Cioslowski, J.; Fox, D. J. *Gaussian 09*, revision A.1; Gaussian, Inc.: Wallingford, CT, 2009. (b) Celani, P.; Robb, M.; Garavelli, M.; Bernardi, F.; Olivucci, M. *Chem. Phys. Lett.* **1995**, *243*, 1.

(22) (a) Orloff, M. K.; Mullen, P. A.; Rauch, F. C. *J. Phys. Chem.* **1970**, *74*, 2189. (b) Borges, I., Jr.; Aquino, A. J. A.; Barbatti, M.; Lischka, H. *Int. J. Quantum Chem.* **2009**, *109*, 2348.

(23) (a) Blancafort, L. *J. Am. Chem. Soc.* **2006**, *128*, 210. (b) Muchova, E.; Slavicek, P.; Sobolewski, A. L.; Hobza, P. *J. Phys. Chem. A* **2007**, *111*, 5259.

(24) Chakraborty, D.; Muller, R. P.; Dasgupta, S.; Goddard, W. A., III. *J. Phys. Chem. A* **2000**, *104*, 2261.

(25) McQuaid, M. J.; Sausa, R. C. *Appl. Spectrosc.* **1991**, *45*, 916.

(26) Levine, R. D. *Molecular Reaction Dynamics*; Cambridge University Press: Cambridge, U.K., 2005; p 264.

(27) Migani, A.; Bearpark, M. J.; Olivucci, M.; Robb, M. *J. Am. Chem. Soc.* **2007**, *129*, 3703.